Electronic states of wires and slabs of topological insulators: Quantum Hall effects and edge transport

L. Brey[1] and H. A. Fertig[2]
[1]*Instituto de Ciencia de Materiales de Madrid, (CSIC), Cantoblanco, 28049 Madrid, Spain*
[2]*Department of Physics, Indiana University, Bloomington, Indiana 47405, USA*
(Received 22 December 2013; published 11 February 2014)

We develop a simple model of surface states for topological insulators, developing matching relations for states on surfaces of different orientations. The model allows one to write simple Dirac Hamiltonians for each surface, and to determine how perturbations that couple to electron spin impact them. We then study two specific realizations of such systems: quantum wires of rectangular cross-section and a rectangular slab in a magnetic field. In the former case, we find a gap at zero energy due to the finite size of the system. This can be removed by application of exchange fields on the top and bottom surfaces, which lead to gapless chiral states appearing on the lateral surfaces. In the presence of a magnetic field, we examine how Landau level states on surfaces perpendicular to the field join onto confined states of the lateral surfaces. We show that an imbalance in the number of states propagating in each direction on the lateral surface is sufficient to stabilize a quantized Hall effect if there are processes that equilibrate the distribution of current among these channels.

DOI: 10.1103/PhysRevB.89.085305 PACS number(s): 72.25.Dc, 73.20.−r, 73.50.−h

I. INTRODUCTION

Topological insulators (TI) are materials with insulating bulks and conducting surfaces. These materials typically are gapped band insulators, where strong spin-orbit coupling has inverted the usual energetic ordering of the bands. Near an interface with the vacuum the bands revert to their usual order, inducing two-dimensional metallic states on their surfaces [1–3]. These surface states have a conical dispersion, and are described by a two dimensional massless Dirac equation centered at a time reversal invariant point in momentum space. The metallic character of these states is protected by time-reversal symmetry, so that a gap can only be opened by perturbations which break this symmetry, e.g., magnetic or exchange fields. Angle-resolved photoemission spectroscopy has confirmed the existence of these surface states in certain materials [4,5].

A magnetic field B applied perpendicular to the surface of the topological insulator quantizes the orbital motion of the electrons and reorganizes the energy spectrum into Landau levels with energies [6–10]

$$E_{\pm} = \pm\sqrt{2n}\hbar\omega_c, \tag{1}$$

where $\omega_c = v_F/\ell$, v_F is the speed of the carriers at the Dirac points in the absence of the field, $\ell = \sqrt{\frac{\hbar c}{eB}}$ is the magnetic length, and $n = 0,1,2,\ldots$. If the Fermi energy of the system passes through the Dirac point for $B = 0$, the corresponding Fermi energy for $B \neq 0$ is pinned in the $n = 0$ Landau level, such that half the states in that level are occupied [11]. Particle-hole symmetry suggests that the Hall conductivity vanishes in this situation. If the Fermi level is raised from this zero point, as it passes between the nth and the $(n+1)$th Landau levels the Hall conductivity from a single surface Dirac point is then quantized to

$$\sigma_{xy} = \left(n + \frac{1}{2}\right)\frac{e^2}{h}\ . \tag{2}$$

In general, the integer quantized Hall effect is associated with current-carrying chiral edge modes. Each mode contributes $\pm e^2/h$ to the Hall conductivity when the Fermi energy passes through it, so one expects only *integer* quantization is possible, in contrast to the bulk result suggested by Eq. (2). The resolution of this discrepancy is that in actual samples, whatever the geometry may be, different surfaces are always connected, and may share edge modes [12–15]. Contacts used to measure the Hall conductance will thus inevitably probe Dirac cones on more than one surface, so that the observed σ_{xy} is always quantized in integer units of e^2/h.

A Hall effect may occur in a system whenever there is time reversal symmetry breaking, so that it may be induced, in principle, without an external applied magnetic field. Doping the system with magnetic impurities, or placing a surface in proximity to a ferromagnetic insulator, which can exchange couple to the TI surface, offer two nonstandard methods to induce $\sigma_{xy} \neq 0$. In such systems, the effective surface Hamiltonian in the absence of such perturbations has the form $H = \hbar v_F(\sigma_x k_y - \sigma_y k_x)$, in which the Pauli matrices σ_x, σ_y represent electron spin operators. In the presence of an exchange field pointing in the $\hat{z}$ direction, a gap opens in the surface spectrum, and a Chern number associated with the states on such a surface has the value $\pm 1/2e^2/h$, with sign determined by the direction of the magnetization [16,17]. This leads to an *anomalous half-integer* contribution of the surface to the Hall conductivity, $\sigma_{xy} = \pm e^2/2h$ [18–20]. As in the usual quantum Hall effect, the existence of multiple surfaces in any real geometry prevents a direct observation of a half-integral quantized Hall conductance in such systems: measured Hall conductances are always integrally quantized. An effect much like this has recently been observed in thin films of $(Bi,Sb)_2Te_2$ doped with Cr atoms [21].

In this work, we introduce a simplified approach to analyzing transport in TI surfaces which are nominally flat, but where surfaces of different orientations may be connected. We show that these simplified surface states give a good accounting of their dispersion within the bulk gap, and develop

matching conditions for surfaces of different orientations. We then apply the formalism first to the problem of a quantum wire with rectangular cross-section, examining the effect of different exchange fields on opposite surfaces. In particular, we find for equal exchange fields that the quantum wire supports gapless chiral states, but when oriented oppositely these states vanish and there is a gap in the spectrum.

In a second application, we consider the quantum Hall problem for a rectangular slab geometry, with field oriented perpendicular to one pair of surfaces. We show that the bulk Landau levels couple surface states on sides parallel to the magnetic field, arriving at results very similar to those of Ref. [14]. We then analyze the effect of phase-breaking processes by contacting the system to equilibrating voltage probes, and argue that in this circumstance the system should support a quantized Hall effect.

This paper is organized as follows. In Sec. II, we introduce the three-dimensional Hamiltonian that describes the low-energy properties of a prototypical TI such as Bi_2Se_3. In Sec. III, we obtain Dirac-like Hamiltonians that describe the various surface states. Section IV is devoted to a discussion of the matching conditions joining states on different surfaces. In Sec. V, we discuss the energy spectrum of the rectangular quantum wire, and Sec. VI discusses what happens to this when exchange fields are introduced on two parallel surfaces. In Sec. VII, we consider the case of TI surfaces in a magnetic field, discuss the energy spectrum in the quantum Hall regime, and then analyze transport in this system in a multiterminal geometry with phase-breaking leads. We conclude with a summary in Sec. VIII.

II. BULK HAMILTONIAN

The properties of three-dimensional topological insulators in the Bi_2Se_3 family of materials can be described by a four band Hamiltonian introduced by Zhang *et al.* [22,23]. In the $\mathbf{k}\cdot\mathbf{p}$ approximation, states near zero energy are controlled by an effective continuum Hamiltonian of the form

$$H^{3D} = E(\mathbf{k}) + \begin{pmatrix} \mathcal{M}(\mathbf{k}) & A_1 k_z & 0 & A_2 k_- \\ A_1 k_z & -\mathcal{M}(\mathbf{k}) & A_2 k_- & 0 \\ 0 & A_2 k_+ & \mathcal{M}(\mathbf{k}) & -A_1 k_z \\ A_2 k_+ & 0 & -A_1 k_z & -\mathcal{M}(\mathbf{k}) \end{pmatrix}, \tag{3}$$

where $\mathcal{M}(\mathbf{k}) = M_0 - B_2(k_x^2 + k_y^2) - B_1 k_z^2$, $k_\pm = k_x \pm i k_y$, and $E(\mathbf{k}) = C + D_1 k_z^2 + D_2(k_x^2 + k_y^2)$. The basis states for which this Hamiltonian is written are $|1\rangle = |p1_z^+, \uparrow\rangle$, $|2\rangle = -i|p2_z^-, \uparrow\rangle$,$|3\rangle = |p1_z^+, \downarrow\rangle$, and $|4\rangle = i|p2_z^-, \downarrow\rangle$, which are hybridized states of the Se p orbitals and the Bi p orbitals, with even (+) and odd (−) parities, and spin up (↑) and down (↓). The Hamiltonian parameters for a particular material can be obtained by fitting to *ab initio* band structure calculations [23]. In the case of Bi_2Se_3, the relevant parameters are $M_0 = 0.28$ eV, $A_1 = 2.2$ eV Å, $A_2 = 4.1$ eV Å, $B_1 = 10$ eV Å^2, $B_2 = 56.6$ eVÅ^2, $C = -0.0068$ eV, $D_1 = 1.3$ eV Å^2, and $D_2 = 19.6$ eV Å^2. In Fig. 1, we plot the band structure of a thick slab of topological insulator with these parameters. The electronic structure is obtained by diagonalizing Eq. (3) with $k_z \to -i\partial_z$, for fixed k_x and k_y, using basis states in which

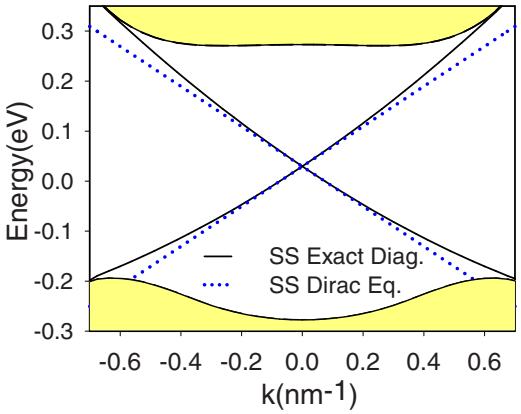

FIG. 1. (Color online) Band structure of a thick TI slab, normal to the $\hat{z}$ direction, as obtained from diagonalizing the Hamiltonian in Eq. (3). Shadow region represents the bulk band structure. The states in the gap correspond to surface states. Dotted lines represent the surface states obtained from the Dirac Hamiltonian (5).

the wave functions to vanish at the surfaces of the slab [24]. The system is rotationally invariant in the x-y plane, so that in Fig. 1, k represents the magnitude of the in-plane momentum.

In what follows, we will be interested in coupling the spin degree of freedom to effective magnetic fields, created by exchange coupling to magnetic insulators or magnetized impurities. To do this, we need the spin operators in the basis of bulk states. These are [25]

$$S_x = \begin{pmatrix} 0 & 0 & 1 & 0 \\ 0 & 0 & 0 & -1 \\ 1 & 0 & 0 & 0 \\ 0 & -1 & 0 & 0 \end{pmatrix},$$

$$S_y = \begin{pmatrix} 0 & 0 & -i & 0 \\ 0 & 0 & 0 & i \\ i & 0 & 0 & 0 \\ 0 & -i & 0 & 0 \end{pmatrix},$$

and

$$S_z = \begin{pmatrix} 1 & 0 & 0 & 0 \\ 0 & 1 & 0 & 0 \\ 0 & 0 & -1 & 0 \\ 0 & 0 & 0 & -1 \end{pmatrix}. \tag{4}$$

We will project these operators onto surface states, yielding operators which depend on the orientation of the surface with respect to the bulk $\mathbf{k}$ axes. It is important to take into account their precise form when analyzing the influence of an effective Zeeman field at such surfaces.

III. SURFACE HAMILTONIANS

An important feature of H^{3D} is that, due to its nontrivial topology, when a surface is introduced one finds states in the gap that can be represented by Dirac Hamiltonians. In this section, we will write down explicit forms for these surface states, following previous approaches [25–27], albeit in a simplified form which allows an introduction of simple

matching conditions between different surfaces. In this work, we consider TI slabs thick enough so that there is not coupling between top and bottom surface states [27–30]. Because of the strong anisotropy of these layered materials, for a given surface the states depend on the orientation of that surface. We confine our analysis to surfaces of high symmetry $(\hat{x},\hat{y},\hat{z})$, and define the surface orientation by normal vectors $\hat{n}=\pm\hat{x}$, $\hat{n}=\pm\hat{y}$, and $\hat{n}=\pm\hat{z}$. Generally speaking, the strategy is to find states which vanish in all its components on the surface, are evanescent as one moves into the bulk of the system, and are constant on planes of constant depth into the bulk. Such states have energies within the bulk gap, and generically one finds two such states which are degenerate. Following the $\mathbf{k}\cdot\mathbf{p}$ approximation, one assumes a good approximation to states near this energy can be formed out of linear combinations of these bound surface states (envelope functions) multiplying plane-wave states with wave vector parallel to the surface, and projects the bulk Hamiltonian, Eq. (3), into the space of these two states. This results in a 2×2 Hamiltonian, with a Dirac spectrum in the absence of other perturbations. Appendix details, as an example, how one obtains the surface Hamiltonian for $\hat{n}_z$. In the following sections, we present the results of such calculations for the three orientations.

A. $\pm\hat{z}$ surface

The Hamiltonian describing the electrons moving on the surface with $\hat{n}=\pm\hat{z}$ has the form

$$H^{\pm\hat{z}}=\frac{D_1}{B_1}M_0\pm A_2\sqrt{1-\frac{D_1^2}{B_1^2}}\begin{pmatrix}0 & ik_x+k_y\\ -ik_x+k_y & 0\end{pmatrix}. \quad (5)$$

This Hamiltonian describes two dimensional Dirac fermions with velocity $v_F=A_2\sqrt{1-\frac{D_1^2}{B_1^2}}$. In Fig. 1, we compare the dispersion obtained from the Dirac Hamiltonian Eq. (5), $\varepsilon=\frac{D_1}{B_1}M_0\pm v_F\sqrt{k_x^2+k_y^2}$, with the exact result obtained from the diagonalization of the 3D Hamiltonian in a thick slab geometry. In the region near the Dirac point, where the dispersion is linear, the Dirac Hamiltonian yields a good description of the surface band structure.

The two states resulting from the solution of the surface problem, which are the envelope functions used in the basis of Eq. (5), are

$$u^{\pm\hat{z}}=\frac{1}{\sqrt{2}}\begin{pmatrix}\sqrt{1+\frac{D_1}{B_1}}\\ \mp i\sqrt{1-\frac{D_1}{B_1}}\\ 0\\ 0\end{pmatrix},\quad v^{\pm\hat{z}}=\frac{1}{\sqrt{2}}\begin{pmatrix}0\\ 0\\ \sqrt{1+\frac{D_1}{B_1}}\\ \pm i\sqrt{1-\frac{D_1}{B_1}}\end{pmatrix}. \quad (6)$$

For this surface orientation, the electron spin operators, formed by projecting the full spin operators [Eq. (4)] onto the two surface states, coincide with the Pauli spin matrices,

$$S_x=\sigma_x,\ S_y=\sigma_y,\ \text{and}\ S_z=\sigma_z. \quad (7)$$

Thus magnetic impurities or the proximity of ferromagnetic insulators will open a gap in the Dirac spectrum only when their magnetization has a component in the $\hat{z}$ direction. As mentioned in Introduction, Eq. (5) in this case picks up a Dirac mass term. The integral of the Berry's curvature in the vicinity of the (now gapped) Dirac point then becomes half integral, and the resulting contribution to the Hall conductivity of electrons in these states is half-integral [16,17].

B. $\pm\hat{x}$ surface

The Hamiltonian describing the electrons moving in the surface perpendicular to the $\pm\hat{y}$ direction has the form

$$H^{\pm\hat{x}}=\frac{D_2}{B_2}M_0\mp\sqrt{1-\frac{D_2^2}{B_2^2}}\begin{pmatrix}A_2k_y & iA_1k_z\\ -iA_1k_z & -A_2k_y\end{pmatrix}. \quad (8)$$

The envelope states forming the basis of this Hamiltonian are

$$u^{\pm\hat{x}}=\frac{1}{\sqrt{2}}\begin{pmatrix}\sqrt{1+\frac{D_2}{B_2}}\\ 0\\ 0\\ \mp i\sqrt{1-\frac{D_2}{B_2}}\end{pmatrix},\quad v^{\pm\hat{x}}=\frac{1}{\sqrt{2}}\begin{pmatrix}0\\ \mp i\sqrt{1-\frac{D_2}{B_2}}\\ \sqrt{1+\frac{D_2}{B_2}}\\ 0\end{pmatrix}. \quad (9)$$

For this surface orientation, the projection of the spin operators in Eq. (4) become

$$S_x=\frac{D_2}{B_2}\sigma_x\ ,\ S_y=\sigma_y\ ,\ S_z=\frac{D_2}{B_2}\sigma_z. \quad (10)$$

The nonintegral coefficients in S_x and S_z arise because the envelope states, Eq. (9), have nonzero amplitudes for microscopic orbitals with different spin orientations. As in the case of the $\pm\hat{z}$ surface, magnetic impurities polarized with a component in the normal direction to the surface open a gap in the Dirac spectrum. Note that for this surface, $S_x\propto\sigma_x$ because of the diagonal term $E(\mathbf{k})$ in Eq. (3); for $D_2=0$, on this surface the component of spin in the x direction will always be zero.

C. $\pm\hat{y}$ surface

The projected states and resulting Hamiltonian for the $\pm\hat{y}$ surfaces are qualitatively very similar to those of the $\pm\hat{x}$ surfaces. The Hamiltonian has the form

$$H^{\pm\hat{y}}=\frac{D_2}{B_2}M_0\pm\sqrt{1-\frac{D_2^2}{B_2^2}}\begin{pmatrix}A_2k_x & -A_1k_z\\ -A_1k_z & -A_2k_x\end{pmatrix}. \quad (11)$$

The envelope states for the states in which the Hamiltonian (11) is expressed are

$$u^{\pm\hat{y}}=\frac{1}{\sqrt{2}}\begin{pmatrix}\sqrt{1+\frac{D_2}{B_2}}\\ 0\\ 0\\ \pm\sqrt{1-\frac{D_2}{B_2}}\end{pmatrix},\quad v^{\pm\hat{y}}=\frac{1}{\sqrt{2}}\begin{pmatrix}0\\ \mp\sqrt{1-\frac{D_2}{B_2}}\\ \sqrt{1+\frac{D_2}{B_2}}\\ 0\end{pmatrix}. \quad (12)$$

Finally, the projections of the spin operators (4) are in this case

$$S_x=\sigma_x,\quad S_y=\frac{D_2}{B_2}\sigma_y,\ \text{and}\ S_z=\frac{D_2}{B_2}\sigma_z. \quad (13)$$

IV. MATCHING CONDITIONS

As discussed in Introduction, in many situations, one cannot understand the transport properties of a TI based on individual surfaces in isolation; it is necessary to understand how these surfaces connect. Towards this end, in this section we develop a simple approach to matching wave functions on a line junction separating two perpendicular surfaces, labeled 1 and 2, of a three-dimensional TI. Our matching method goes beyond the simple approximation of matching the wave-function components without considering how these amplitudes relate to the underlying bulk Hamiltonian [31,32]. We assume the Fermi energy is in a bulk gap and focus on how these matching conditions impact the surface state spectra and associated conduction properties. Our method uses a general approach [33], in which wave functions of a system are matched along some chosen surface that divides the system into disparate pieces, each having different transverse modes into which it is natural to decompose wave functions. In principle, the matching can be carried out precisely by considering overlaps along the chosen surface of all the transverse modes. In practice, it is usually necessary to truncate the number of modes kept, allowing one to obtain approximate results for wave functions in some energy interval. This general approach has been quite successful for treating semiconductor nanostructures [33] and, recently, has been useful for understanding transport through graphene nanostructures [34].

In the present context, we are interested in understanding spectra and transport when there are only a small number of modes crossing the Fermi energy, with wave functions confined to the surfaces, while all other transverse modes (associated with the bulk) represent states well above or below the Fermi energy. These latter states are incorporated as evanescent states which do not directly contribute to the current in the system, although they quantitatively affect the scattering among conducting modes. The simplest approximation in this situation is to ignore the evanescent modes entirely, leading to an "open mode approximation" [33]. However, this does not define the approximation scheme uniquely, as one may choose the matching surface to obtain the best results. Below we demonstrate that demanding that the truncated Hamiltonian be Hermitian effectively singles out a specific set of matching conditions within the open mode approximation.

A. Open mode approximation

To motivate our matching conditions, it is useful to consider two slabs of the TI system, with surface normals perpendicular to one another, joined through a perpendicular junction. Figure 2 illustrates the corner of such a junction, emphasizing the role of the surface states, which are most important when the Fermi energy is in the bulk gap. For concreteness, we assume one of these has horizontal surfaces, perpendicular to $\hat{z}$, and the other vertical surfaces perpendicular to $\hat{x}$. Assuming that the system is uniform along the $\hat{y}$ direction so that k_y is a good quantum number, states of the first slab can be written in the form $\Psi^{(z)} = e^{ik_y y}\sum_n e^{ik_x^{(n)}x}c_n^{(z)}\chi_n^{(z)}(z)$, and for the second slab $\Psi^{(x)} = e^{ik_y y}\sum_n e^{ik_z^{(n)}z}c_n^{(x)}\chi_n^{(x)}(x)$. In these expressions, $\chi_n^{(z,x)}$ are transverse wave functions for the slabs, among which are the surface states discussed in the last section [35] and for this problem are four component vectors; the wave vectors $k_{x,z}^{(n)}$ are determined by the energy of the state, and in most cases are actually complex (i.e., represent evanescent states) if the Fermi energy is in the bulk band gap, and the coefficients $c_n^{(x,z)}$ are weights which must be related by appropriate matching conditions. This last requirement in principle can be implemented by matching all components of the wave functions on some surface along which the two slabs are joined together. In principle, one may choose any convenient surface, and parametrize it as (x_λ, z_λ), with $0 \leqslant \lambda \leqslant 1$. For a given set of coefficients on one side of the junction, say $\{c_n^{(z)}\}$, the coefficients on the other side can, in principle, be found [33] by a matrix multiplication, $c_n^{(x)} = \sum_m \langle x,n|z,m\rangle c_m^{(z)}$ with

$$\langle x,n|z,m\rangle = \int_{\lambda=0}^{\lambda=1} ds_\lambda e^{-ik_z^{(n)}z_\lambda + ik_x^{(m)}x_\lambda}\langle \chi_n^{(x)}(x_\lambda)|\chi_m^{(z)}(z_\lambda)\rangle.$$

Here, ds_λ is the differential arc length along the joining surface, and $\langle \chi_n^{(x)}(x)|\chi_m^{(z)}(z)\rangle$ is the dot product of the four component vectors.

In general, the challenge in carrying out this matching is that the full matrix $\langle x,n|z,m\rangle$ is difficult to compute. Moreover, typically most of the transverse modes are "closed"—i.e., they host evanescent states—and do not contribute directly to current across the junction. In the "open mode" approximation one simply ignores the closed modes and retains only those that are current-carrying at the Fermi energy. In the present context, this is particularly simplifying since only the surface modes are open when the Fermi energy is in the bulk gap.

In the present case it is then natural to retain only the u and v modes detailed in the last section. If one further assumes that the penetration depths of the surface states (λ_1 and λ_2 in Appendix) are short, such that the phase factor $e^{-ik_z^{(n)}z_\lambda + ik_x^{(m)}x_\lambda}$ has a negligible variation on the joining surface in the region where $\langle \chi_n^{(x)}(x_\lambda)|\chi_m^{(z)}(z_\lambda)\rangle$ is significantly different than zero, the resulting connection between coefficients takes the simple form

$$\begin{pmatrix} c_u^x \\ c_v^x \end{pmatrix} = M_{x,z}\begin{pmatrix} c_u^z \\ c_v^z \end{pmatrix}, \tag{14}$$

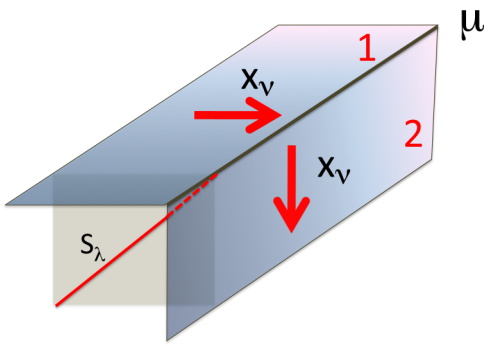

FIG. 2. (Color online) Junction between two perpendicular surfaces, 1 and 2 of a three-dimensional TI. The direction of the line junction is μ. x_ν indicates the effective one dimensional coordinate in the surfaces 1 and 2. s_λ parameterizes a curve perpendicular to μ (here a straight line) on the surface joining the two slabs at a corner junction.

where we have written the two open channel coefficients for each surface c_n^μ with $n \to u,v$. The matrix $M_{x,z}$ has the form

$$M_{x,z} = \mathcal{C}_{xz}\begin{pmatrix} \gamma_+ & \gamma_- \\ -\gamma_- & \gamma_+ \end{pmatrix} \tag{15}$$

with

$$\gamma_\pm = \sqrt{[(1 \pm D_1/B_1)(1 \pm D_2/B_2)]},$$

and $\mathcal{C}_{xz} = \int ds_\lambda [e^{\lambda_1^x x_\lambda} - e^{\lambda_2^x x_\lambda}][e^{\lambda_1^z z_\lambda} - e^{\lambda_2^z z_\lambda}]$, with $\lambda_{(1,2)}^{(x,z)}$ the corresponding $\lambda_{(1,2)}$ constants in Appendix.

At this level of approximation, the only relevant information about the joining surface is contained in the constant $\mathcal{C}_{xz}$. We thus will ultimately choose this constant—implicitly, by choosing the joining surface—to obtain the best approximation, which we will argue below leaves the projected Hamiltonian Hermitian; this choice uniquely fixes the value of the constant. Before turning to this, we summarize the results of the open mode approximation for other possible 90° corner junctions with surfaces normal to principal axes of the structure. In general, we write

$$\begin{pmatrix} c_u^\mu \\ c_v^\mu \end{pmatrix} = M_{\mu,\nu}\begin{pmatrix} c_u^\nu \\ c_v^\nu \end{pmatrix}, \tag{16}$$

with $\mu,\nu = x,y,z$, and

$$\begin{aligned}
M_{z,x} &= M_{-z,-x} = \mathcal{C}_{xz}\begin{pmatrix} \gamma_+ & \gamma_- \\ -\gamma_- & \gamma_+ \end{pmatrix}, \\
M_{-z,x} &= M_{z,-x} = \mathcal{C}_{zx}\begin{pmatrix} \gamma_+ & -\gamma_- \\ \gamma_- & \gamma_+ \end{pmatrix}, \\
M_{z,y} &= M_{-z,-y} = \mathcal{C}_{yz}\begin{pmatrix} \gamma_+ & i\gamma_- \\ i\gamma_- & \gamma_+ \end{pmatrix}, \\
M_{z,-y} &= M_{-z,y} = \mathcal{C}_{zy}\begin{pmatrix} \gamma_+ & -i\gamma_- \\ -i\gamma_- & \gamma_+ \end{pmatrix}, \\
M_{\pm x,\pm y} &= \mathcal{C}_{xy}\begin{pmatrix} 1 & 0 \\ 0 & 1 \end{pmatrix}.
\end{aligned} \tag{17}$$

B. Hermitian effective Hamiltonian

As discussed above, we would like to choose the $\mathcal{C}_{\mu,\nu}$ coefficients to optimize the approximation. In particular, in order to obtain sensible results within the approximation scheme, the projected Hamitonian of the full system should be Hermitian. This guarantees among other things that current will be conserved across the junctions. We now show that this requirement uniquely fixes the coefficients $\mathcal{C}_{\mu,\nu}$.

As a concrete example we return to the geometry illustrated in Fig. 2. The system is invariant along the $\hat{y}$ direction, so that we can consider the system for each k_y as one-dimensional, with a single coordinate along the surface, running perpendicular to the line junction. The corner can be "flattened" by taking $x < 0$ to represent the $\hat{z}$ surface, and $x > 0$ to represent the $\hat{x}$ surface, which we refer to respectively as the 1 and 2 surfaces in what follows. In this notation, the portion of the low-energy Hamiltonian, which represents the problem, has the form

$$h_x = i\hbar A(x)\sigma_y \partial_x \,. \tag{18}$$

$A(x)$ is piecewise constant but jumps at $x = 0$. Potentially, this leads to problems because matrix elements between arbitrary two-component wave functions $\phi_1(x)$ and $\phi_2(x)$ may not obey $\int dx \phi_1^* h_x \phi_2 = \int dx (h_x \phi_1)^* \phi_2$ due to a surface term at $x = 0$ from integration by parts. In particular [14], the Hamiltonian is only Hermitian if

$$A^+ \phi_1^{-\dagger} \sigma_y \phi_2^- = A^- \phi_1^{+\dagger} \sigma_y \phi_2^+, \tag{19}$$

where $A^\pm \equiv A(x = 0^\pm)$ and $\phi_{1,2}^\pm \equiv \phi_{1,2}(0^\pm)$. From Eq. (14), this means

$$A^+ \phi_1^{-\dagger} \sigma_y \phi_2^- = A^- \phi_1^{+\dagger} \sigma_y M_{xz} \phi_2^-,$$

from which we read off

$$A^+ \phi_1^{-\dagger} \sigma_y = A^- \phi_1^{+\dagger} \sigma_y M_{xz}.$$

Taking the Hermitian conjugate of this yields

$$A^+ \sigma_y \phi_1^- = A^- M_{xz}^\dagger \sigma_y \phi_1^+,$$

and since $\phi_1^+ = M_{xz}\phi_1^-$, we arrive at the relation

$$\frac{A^+}{A^-} = \sigma_y M_{xz}^\dagger \sigma_y M_{xz}. \tag{20}$$

From the form of Eq. (15), we see $M_{x,z} = \mathcal{C}_{xz}(\gamma_+ + i\gamma_-\sigma_y)$, and plugging this into Eq. (20) above, we arrive at the condition

$$\mathcal{C}_{xz}^2 = \frac{A^+}{A^-}(\gamma_+^2 + \gamma_-^2)^{-1}. \tag{21}$$

For the xz line junction, $A^+ = A_1$ and $A^- = A_2$.

Equation (21) uniquely specifies the matching condition we should use in an open mode approximation to get physically sensible results. It is interesting to note that if one sets $\phi_1 = \phi_2$ in Eq. (19), the resulting condition is precisely what is needed to get current conservation across the junction. Finally, generalizing this result to other corner junctions, we find

$$\begin{aligned}
\mathcal{C}_{zx}^2 &= \frac{A_2}{A_1}(\gamma_+^2 + \gamma_-^2)^{-1}, \\
\mathcal{C}_{yx}^2 &= \frac{A_1}{A_2}(\gamma_+^2 + \gamma_-^2)^{-1}, \\
\mathcal{C}_{zy}^2 &= \frac{A_2}{A_1}(\gamma_+^2 + \gamma_-^2)^{-1}, \\
\mathcal{C}_{xy} &= 1.
\end{aligned} \tag{22}$$

V. TOPOLOGICAL INSULATOR QUANTUM WIRE

As a first example of how these matching conditions can be used, we analyze the electronic structure of the surface states of a quantum wire (QW) with rectangular cross section. For this example, we neglect the diagonal term $E(\mathbf{k})$ in Hamiltonian (3), which breaks electron-hole symmetry. This allows us to obtain analytical results, which are easily understood.

The dimensions of the QW are L_x and L_z along the x and z axes, respectively, and it is infinitely long in the $\hat{y}$ direction, so that k_y is a good quantum number. Given the momentum k_y and the energy E, for each surface of the QW ($\pm x, \pm z$), one may find the corresponding electron wave functions ($\Psi^{\pm x,\pm z}$), each as a linear combination of the two solutions of the corresponding Dirac-like surface Hamiltonians. Thus there

are eight coefficients that determine the QW wave function, which obey four equations of the form in Eq. (16). Explicitly, we define two-component wave functions of the form

$$\varphi^{(+z)}(x) = \begin{pmatrix} c_u^{(+z)} \\ c_v^{(+z)} \end{pmatrix}_{+k_x} A^{(+z)} e^{ik_x x} + \begin{pmatrix} c_u^{(+z)} \\ c_v^{(+z)} \end{pmatrix}_{-k_x} B^{(+z)} e^{-ik_x x},$$

$$\varphi^{(+x)}(z) = \begin{pmatrix} c_u^{(+x)} \\ c_v^{(+x)} \end{pmatrix}_{+k_z} A^{(+x)} e^{ik_z z} + \begin{pmatrix} c_u^{(+x)} \\ c_v^{(+x)} \end{pmatrix}_{-k_z} B^{(+x)} e^{-ik_z z},$$

$$\varphi^{(-z)}(x) = \begin{pmatrix} c_u^{(-z)} \\ c_v^{(-z)} \end{pmatrix}_{+k_x} A^{(-z)} e^{ik_x x} + \begin{pmatrix} c_u^{(-z)} \\ c_v^{(-z)} \end{pmatrix}_{-k_x} B^{(-z)} e^{-ik_x x},$$

$$\varphi^{(-x)}(z) = \begin{pmatrix} c_u^{(-x)} \\ c_v^{(-x)} \end{pmatrix}_{+k_z} A^{(-x)} e^{ik_z z} + \begin{pmatrix} c_u^{(-x)} \\ c_v^{(-x)} \end{pmatrix}_{-k_z} B^{(-x)} e^{-ik_z z},$$

where k_x is the value that, when substituted into Eq. (5), yields a particular energy eigenvalue E, k_z is the analogous value for Eq. (8), $(c_u^{(\mu)*}\, c_v^{(\mu)*})^\dagger_{\pm k_y}$ are the normalized eigenvectors of these Hamiltonians, and $A^{(\pm\mu)}$, $B^{(\pm\mu)}$ are coefficients which must be determined by matching at the corners. These matching conditions are

$$\begin{aligned} \varphi^{(+z)}(x=0) &= M_{z,x}\, \varphi^{(+x)}(z=0), \\ \varphi^{(-z)}(x=0) &= M_{-z,x}\, \varphi^{(+x)}(z=-L_z), \\ \varphi^{(-z)}(x=-L_x) &= M_{-z,-x}\, \varphi^{(-x)}(z=-L_z), \\ \varphi^{(+z)}(x=-L_x) &= M_{z,-x}\, \varphi^{(-x)}(z=0). \end{aligned} \tag{23}$$

For a given momentum k_y, the matching conditions can only all be met at particular energies $E = \epsilon_{n,k_y}$ that define the QW band structure. If we neglect $E(\mathbf{k})$ in Eq. (3), it is possible after some algebra to find these energies analytically, with the result

$$\epsilon_{n,k_y} = \pm\sqrt{(A_2 k_y)^2 + \left[\pi \frac{A_1 A_2}{A_1 L_z + A_2 L_x}\left(n - \frac{1}{2}\right)\right]^2}, \tag{24}$$

with $n = 1,2,3\ldots$, and we have made the further simplifying assumption that $B_1 = B_2 = D_1 = D_2 = 0$. This band structure is spin degenerate.

Equation (24) can be easily rationalized with a geometrical argument. When a carrier moves in a closed loop around the quantum wire, the matching of the wave functions yields the quantization condition

$$2(k_x L_x + k_z L_z) + \pi = 2\pi n\,. \tag{25}$$

The phase π in the left part of the quantization equation appears because of the helical nature of the carriers: when the electrons encircle the QW, the expectation value of the Pauli matrices that appear in the Dirac Hamiltonians rotates by 2π, so that the wave function acquires a Berry phase of π. (An analogous accumulation of phases occurs in graphene hexagonal quantum rings with discrete 120° corners [36].) Moreover, the wave vectors k_z and k_x are related to the energy by

$$E = \sqrt{(A_1 k_z)^2 + (A_2 k_y)^2} = \sqrt{(A_2 k_x)^2 + (A_2 k_y)^2}\,. \tag{26}$$

Combining Eqs. (25) and (26), one obtains the band structure Eq. (24).

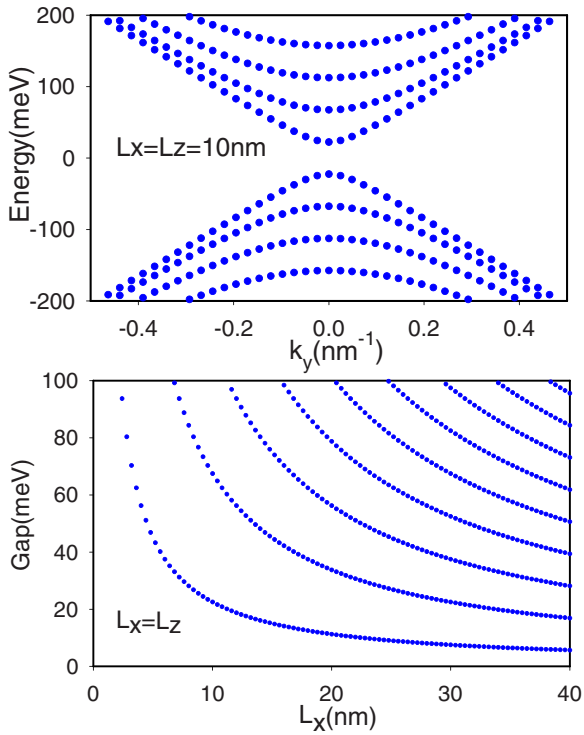

FIG. 3. (Color online) (Top) Band structure of a TI QW with $L_z = L_x = 10$ nm, as obtained from Eq. (24). (Bottom) Dependence of the $k_y = 0$ energy levels on the dimensions of the TI QW.

In Fig. 3, we plot the band structure as a function of the momentum k_y for a QW with $L_z = L_x = 10$ nm, and the dependence of the $k_y = 0$ energy levels on the dimensions of the QW. Analogous band structures for a TI QW have been obtained in a cylindrical geometry [37,38].

VI. EXCHANGE FIELDS AND ANOMALOUS QUANTUM HALL EFFECT

Interesting physics can be induced in these types of systems by the introduction of time-reversal symmetry breaking perturbations on the surfaces. As discussed in Introduction, this can be accomplished by thin-film ferromagnets, exchange coupled to one or more surfaces of the system. In particular, these can couple to the spin of the electrons without introducing orbital magnetic flux into the Hamiltonian.

For a single such surface, for example, with normal in the $\pm\hat{z}$ direction, an exchange field $\vec{\Delta}$ parallel to this opens an energy gap [see Eqs. (5)–(7)]. By contrast, if the surface has normal perpendicular to $\vec{\Delta}$, the spectrum remains gapless [see Eqs. (8)–(10)]. An isolated gapped surface appears to support an *anomalous* half integer Hall conductivity $\sigma_{xy} = \mathrm{sign}(\Delta)\frac{1}{2}\frac{e^2}{h}$. As discussed in Introduction, in real geometries for which there must be a top and bottom surface, the Hall conductivity becomes integrally quantized.

In this section, we analyze a TI quantum wire of rectangular section in presence of a z-polarized exchange field. Δ enters as a mass term in the Dirac Hamiltonians for the $\pm\hat{z}$ surfaces, but does not qualitatively modify the Hamiltonians corresponding to the $\pm\hat{x}$ and $\pm\hat{y}$ surfaces. Again, in order to simplify the

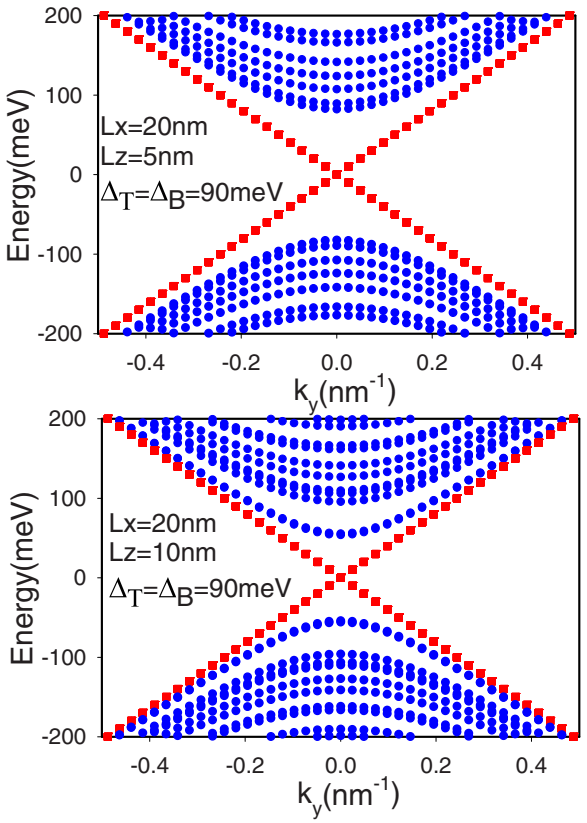

FIG. 4. (Color online) Energy bands of a TI QW in presence of equal exchange fields $\Delta_T = \Delta_B = 90$ meV in top and bottom surfaces. Blue circle points are not chiral states, while red squares correspond to chiral states. Dimensions of the QW are $L_x = 20$ nm and $L_z = 5$ nm (10 nm), in the top (bottom) panel.

discussion, we neglect in the Hamiltonian terms proportional to D_1 and D_2.

Figure 4 illustrates the energy spectrum of a TI QW with lateral dimensions $L_z = 20$ nm and $L_z = 5$ nm (top panel) and $L_z = 10$ nm (bottom panel) in the presence of an exchange field of magnitude 90 meV. There are three kinds of states. (i) For energies smaller than $\sqrt{\Delta^2 + A_2^2 k_y^2}$, there are states confined to the lateral surfaces, with energies below the gap for states on the exchange-coupled surfaces. The energies of these states depend on the lateral size L_z of the wire. For the values of L_z and Δ illustrated in Fig. 4, tunneling between states on opposite lateral surfaces is essentially negligible, so that these states are nearly doubly degenerate; deviations from this are only apparent at energies very close to Δ. (ii) At energies larger than Δ the states extend along the entire perimeter of the TI QW. Because time reversal symmetry is broken by the exchange field, these states are not degenerate. (iii) Finally, there gapless modes with linear dispersion $\pm A_2 k_y$. These describe chiral states moving in opposite directions on opposite lateral surfaces.

States of type (i) and (ii) are not chiral: for each state there is a counter-propagating state on the same surface. Impurities can induce backscattering among these states and lead to localization. Chiral states moving in opposite directions reside on opposite surfaces, and for a wide enough system, backscattering is negligible. Magnetically gapped top and bottom surfaces are always connected by surfaces with these chiral states, so that the *anomalous* Hall conductivity of the system as a whole is e^2/h.

To gain more insight into the nature of the chiral states, we look for a criterion that determines when they are present. Consider a system in which the top and layers are perturbed by exchange fields Δ_T and Δ_B, respectively. We look for wave functions on a single lateral surface with momentum k_z=0, and energy $E = sA_2k_y$, with $s = \pm 1$. In this geometry, the top and bottom wave functions (extending into the x-y plane with $x < 0$) and the lateral wave function (at $x = 0$) have the form

$$\begin{aligned}
\varphi^{(+z)} &= C \begin{pmatrix} 1 \\ \frac{sA_2k_y - \Delta_T}{A_2k_y + |\Delta_T|} \end{pmatrix} e^{|\Delta_T|x}, \\
\varphi^{(-z)} &= C' \begin{pmatrix} -1 \\ \frac{sA_2k_y - \Delta_B}{A_2k_y + |\Delta_B|} \end{pmatrix} e^{|\Delta_T|x}, \\
\varphi^{(x)} &= \alpha \begin{pmatrix} 1-s \\ 1+s \end{pmatrix} + \beta \begin{pmatrix} 1-s \\ 1+s \end{pmatrix}.
\end{aligned} \tag{27}$$

Solutions with energy $\pm sA_2k_y$ will exist if these wave functions satisfy the boundary conditions Eq. (16) at the matching points $(x = 0, z = 0)$ and $(x = 0, z = -L_z)$,

$$\begin{aligned}
C \begin{pmatrix} 1 \\ \frac{sA_2k_y - \Delta_T}{A_2k_y + |\Delta_T|} \end{pmatrix} &= \begin{pmatrix} \alpha + \beta \\ s(\alpha + \beta) \end{pmatrix}, \\
C' \begin{pmatrix} -1 \\ \frac{sA_2k_y - \Delta_B}{A_2k_y + |\Delta_B|} \end{pmatrix} &= \begin{pmatrix} -(\alpha + \beta)s \\ \alpha + \beta \end{pmatrix}.
\end{aligned} \tag{28}$$

For top and bottom exchange fields with the same sign, the boundary conditions are only satisfied for $s = -1$. Therefore, in the lateral surface (normal to $\hat{x}$ direction), there is a chiral state where the electrons move in the $-\hat{y}$ direction with speed A_2. Similar equations can be written for the opposite lateral surface, normal to the $-\hat{x}$ direction, where the band dispersion is A_2k_y, and the chiral carriers also move in the $\hat{y}$ direction with speed A_2, albeit in the opposite direction.

Finally, it is interesting to see what happens to this picture when the exchange fields on the top and bottom surfaces point in opposite directions, $\vec{\Delta}_T \cdot \vec{\Delta}_B < 0$. In this case, Eq. (28) has no solutions, and chiral states are not present in the system. Figure 5 illustrates a full solution of the problem as described in the last section, corroborating this structure. This is consistent with general considerations in terms of the surface Chern numbers: the top and bottom surfaces have Chern number $\pm 1/2$, so that the system as a whole has Chern number zero. In this situation (and in the absence of gapless lateral states), the system does not exhibit an anomalous quantized Hall effect.

VII. LANDAU LEVELS, EDGE STATES, AND QUANTUM HALL EFFECT IN A TI SLAB

A. Energy spectrum

In this section, we study the electronic band structure of a TI slab in the presence of a perpendicular magnetic field B. The magnetic field points in the $\hat{z}$ direction and does not affect the motion of electrons on surfaces where this is in the plane.

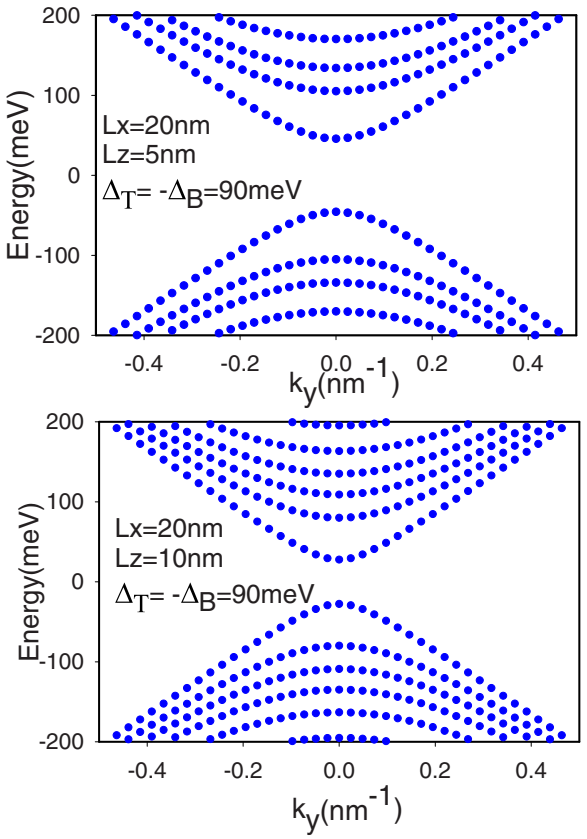

FIG. 5. (Color online) Energy bands of a TI QW in presence of exchange fields of opposite sign in the top and bottom surfaces, $\Delta_B = -\Delta_T = 90$ meV. In this configuration, the total Chern number is zero and there are no chiral states. Dimensions of the QW are $L_x = 20$ nm and $L_z = 5$ nm (10 nm), in the top (bottom) panel.

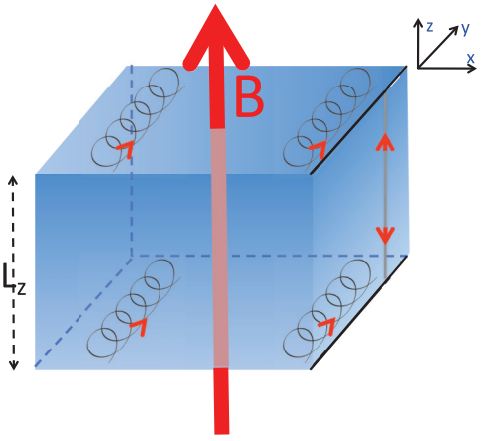

FIG. 6. (Color online) Schematic diagram of a semi-infinite thin slab of TI in presence of a perpendicular magnetic field. The slab, of thickness L_z, is perpendicular to the $\hat{z}$ direction, invariant in the $\hat{y}$ direction and it is defined for $x < 0$. Carriers in the top and bottom surfaces are in the same magnetic field, whereas electrons in the lateral surface are not affected by it. When the guiding center of the electron motion is located away from the edge of the sample, the electronic wave functions of the top and bottom surfaces are those of bulk Landau levels. When a guiding center approaches the edge, wave functions on top and bottom surfaces become coupled through lateral surface plane waves states.

We choose the Landau gauge $\mathbf{A} = (0, -Bx, 0)$, which does not depend on the coordinate y, so that the wave vector k_y is a good quantum number. In what follows, we again neglect the diagonal terms involving $E(\mathbf{k})$ in the three dimensional Hamiltonian (3). Adopting $A_2\ell^{-1}$ as our unit of energy and $\ell = \sqrt{\hbar c/eB}$ as our unit of length, the Hamiltonian (5) in the presence of the magnetic field takes the form

$$H^{\pm z} = \pm \begin{pmatrix} 0 & -\sqrt{2}\partial_z + \frac{z}{\sqrt{2}} \\ +\sqrt{2}\partial_z + \frac{z}{\sqrt{2}} & 0 \end{pmatrix}, \qquad (29)$$

with $z = \sqrt{2}(k_y - x)$. The eigenvectors $(\phi_1^{\pm}, \phi_2^{\pm})$ of Eq. (29) are obtained by squaring the eigenvalue equation $H^{\pm z}\phi = E\phi$, yielding

$$\left(\partial_z^2 - \frac{z^2}{4} + \frac{E^2}{2} + \frac{1}{2}\right)\phi_1 = 0, \qquad (30)$$

$$\left(\sqrt{2}\partial z + \frac{z}{\sqrt{2}}\right)\phi_1 = \pm\phi_2\,. \qquad (31)$$

Solutions of the above equations that do not diverge at $x \to -\infty$ are

$$\begin{pmatrix} \phi_1^{\pm} \\ \phi_2^{\pm} \end{pmatrix} = \alpha \begin{pmatrix} D_{\frac{E^2}{2}}[\sqrt{2}(k_y - x)] \\ \pm\frac{E}{\sqrt{2}} D_{\frac{E^2}{2}-1}[\sqrt{2}(k_y - x)] \end{pmatrix}, \qquad (32)$$

where $D_p(z)$ are parabolic cylinder functions [39]. Carriers moving on the lateral surface $\hat{x}$ are not affected by the magnetic field so that the wave functions are eigenstates of the Hamiltonian in Eq. (8). By matching of these lateral wave functions with those on the top and bottom surfaces we obtain the band structure of a semi-infinite TI slab in presence of the magnetic field. The geometry is illustrated schematically in Fig. 6.

In Fig. 7, we plot the results of such a calculation [40]. For large and negative momentum k_y, the guiding center of the electron orbits, $k_y\ell^2$, is located well inside the top and bottom surfaces where there is a uniform magnetic field, and the coupling to the lateral surface is very small. The spectrum then consists of double degenerate Landau levels, one each for the top and bottom layers, with energies $\pm\sqrt{2n}A_2\ell^{-1}$. As k_y increases, approaching zero from below, the Landau level wave functions approach and acquire non-negligible coupling to the lateral surface states. For the nth Landau level, when $-k_y\ell \sim \sqrt{2|n|}$, this coupling becomes important and, for $|n| > 0$, the absolute value of the energy decreases. This occurs because the wave function penetrates into the (zero-field) lateral surface, where the carriers can have a smaller kinetic energy than in the presence of the field [41]. The $n = 0$ Landau levels of the top and bottom surfaces behave differently because they carry no kinetic energy. When the guiding center approaches the junction with the lateral surface, coupling between them becomes important and they form bonding and antibonding states with the accompanying level repulsion. For $k_y\ell^2$ well inside the lateral surface, one finds bound states due to its finite width in the $\hat{z}$ direction; the energy spacing between these states scales as $1/L_z$ [14]. Increasing the width of the lateral surface (i.e., the separation between top and bottom

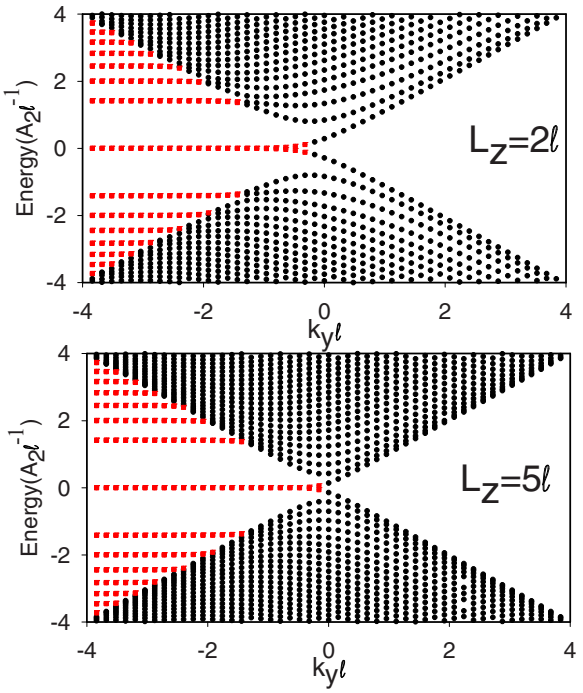

FIG. 7. (Color online) Energy spectrum of a TI slab of thickness $L_z = 2\ell$ (top) and 5ℓ (bottom). Red square points correspond to wave functions that are mainly located in the top and bottom layers and decay exponentially in the lateral surfaces. For $k_y\ell \ll -1$, these states evolve into bulk Landau levels. For large values of $-k_y\ell$, the top and bottom surfaces Landau levels are degenerate. For $k_y\ell \gtrsim -l$, top and bottom Landau levels couple through the lateral states and the degeneracy is lifted. Black dot points correspond to states confined in the lateral surfaces. The energy spacing of these states scale as $1/L_z$ [14].

surfaces) generates more lateral bound states, but does not affect the separation between Landau levels.

The discussion above neglects the coupling of the electron spin to the magnetic field. In the $\pm\hat{z}$ surfaces, there is an additional Zeeman coupling, so the Landau level energies become

$$E_\pm = \pm\sqrt{(2A_2\ell^{-1}n)^2 + E_Z^2}, \tag{33}$$

where $E_Z = g\mu_B B/2$, with μ_B the Bohr magneton and g the effective Landé factor. Note that in some topological insulators, this last quantity can be as much as fifty times larger than for free electrons [42]. In Fig. 8, we plot the band structure for a Zeeman coupling $E_z = 0.2A_2\ell^{-1}$. The main effects of the Zeeman coupling are to break the electron-hole symmetry, shift the energies of the Landau levels, and to lift the degeneracy between the $n = 0$ Landau levels.

B. Quantum Hall effect

The presence of many counterpropagating channels on the lateral surfaces can have important consequences for the quantization of the Hall conductance in this system. When the chemical potential is between Landau levels, for example, as in the spectra illustrated in Fig. 7, it is apparent that the number of left- and right-moving channels crossing the Fermi

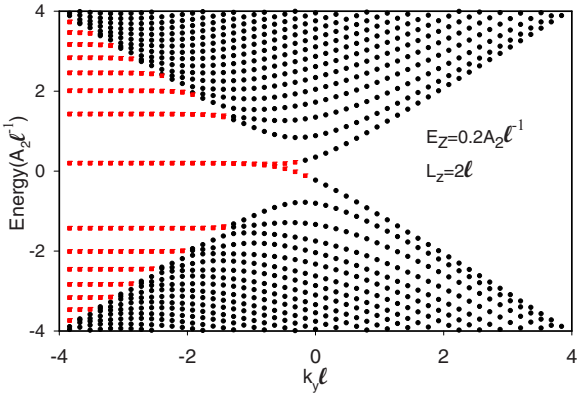

FIG. 8. (Color online) Energy spectrum of a TI slab of thickness $L_z = 2\ell$ with an orbital B-field as in Fig. 7 and a Zeeman field coupling with energy $E_z = 0.2A_2\ell^{-1}$.

energy are not equal. If there are $N + M$ channels propagating in one direction and N channels propagating in the other on each lateral surface, when the transport on these surfaces is ballistic, the Hall conductance does *not* turn out to be simply Me^2/h [14]. Moreover, the longitudinal resistance on one of the lateral surfaces does not vanish. In these circumstances, the system does not exhibit a quantized Hall effect.

The absence of a quantized Hall effect in these circumstances can be understood as due to the fact that when current is injected into the system from an ideal lead, since only channels with current directed away from the lead can absorb this current, the distribution of currents among the channels is out of equilibrium. This suggests that the system will support a quantized Hall effect if there are current-conserving mechanisms by which this distribution can relax. Generically, this will be the case in real systems.

As a simple model, we consider a geometry as illustrated in Fig. 9, which uses phase-breaking voltage probes to equilibrate the populations at the edges [43,44]. The voltage probes absorb current from each channel with probability Γ, taken to be the same for all the channels. Since voltage probes do not change the current down the lateral surface, the total current

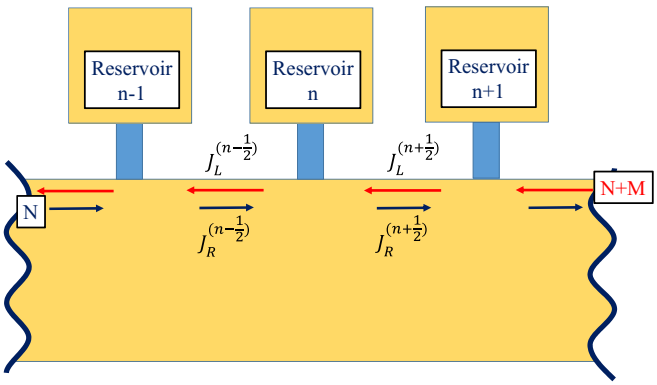

FIG. 9. (Color online) Model of TI slab edge connected to equilibrating leads. Sample edge supports N right-moving and $N + M$ left-moving channels. Left (right)-moving current between reservoirs $n - 1$ and n is labeled as $J_{L(R)}^{(n-1/2)}$.

absorbed by each probe is also emitted from a reservoir at some chemical potential μ_n. The current is assumed to be injected into each of the lateral channels with equal probability. In this way, the voltage probes have the effect of relaxing the current into an equilibrium distribution. Although one can include backscattering among channels at the edge due the leads as well as quantum interference among the various edge and voltage probe channels in such a model [43], we ignore these possibilities to focus on phase-breaking effects.

Defining left-moving and right-moving currents between leads $n-1$ an n as $J^{(L)}_{n-1/2}$ and $J^{(R)}_{n-1/2}$, respectively, the current entering reservoir n has the form $[J^{(R)}_{n-1/2}+J^{(L)}_{n+1/2}]\Gamma$. Current not absorbed from a channel continues onto the next interval between reservoirs. With the assumption that the reservoir returns all the current it absorbs back into the lateral surface with equal probability among the outgoing channels, one finds

$$J^{(R)}_{n+1/2} = (1-\Gamma)J^{(R)}_{n-1/2} + \frac{N}{2N+M}\Gamma\left(J^{(L)}_{n+1/2}+J^{(R)}_{n-1/2}\right),$$
$$J^{(L)}_{n-1/2} = (1-\Gamma)J^{(L)}_{n+1/2} + \frac{N+M}{2N+M}\Gamma\left(J^{(L)}_{n+1/2}+J^{(R)}_{n-1/2}\right). \tag{34}$$

Note this set of equation guarantees that the net current $J^{(R)}_{n+1/2}-J^{(L)}_{n+1/2}$ will be the same for all intervals n. They can be recast into a recursion relation of the form

$$\begin{pmatrix} J^{(R)}_{n+1/2} \\ J^{(L)}_{n+1/2} \end{pmatrix} = T \begin{pmatrix} J^{(R)}_{n-1/2} \\ J^{(L)}_{n-1/2} \end{pmatrix} \tag{35}$$

with

$$T = \frac{1}{1-\gamma N}\begin{pmatrix} 1-\gamma(2N+M) & \gamma N \\ -\gamma(N+M) & 1 \end{pmatrix}, \tag{36}$$

where $\gamma = \Gamma/(2N+M)$.

This recursion relation allows one to determine the currents on the top edge, as illustrated in Fig. 9, anywhere down the length of the sample, provided the current far to the left of the system is known. An analogous relation can be written for the bottom edge, whose currents depend on a boundary condition on the right. These boundary conditions are met at current-injecting contacts (not shown in the figure, on lateral surfaces perpendicular to the one illustrated), and determine how the net current down the Hall bar divides between the top and bottom lateral surfaces.

Because the transfer matrix T is independent of n, one may straightforwardly determine the distribution of current in the left-moving and right-moving channels, $\vec{J}_{n+1/2} = (J^{(R)}_{n+1/2}, J^{(L)}_{n+1/2})^\dagger$, by expressing these in terms of the eigenvectors of T, $\vec{J}_{0,t} \equiv (J^{(R)}_{0,t}, J^{(L)}_{0,t})^\dagger$, where the corresponding eigenvalues are $\lambda_0 = 1$ and $\lambda_t = 1-\gamma M/(1-\gamma N)$: $\vec{J}_{n+1/2} = a_0\lambda_0^n\vec{J}_0 + a_t\lambda_t^n\vec{J}_t$. The amplitudes $a_{0,t}$ are determined by the boundary conditions mentioned above. Since $\lambda_t < 1$, the component of currents associated with $\vec{J}_t$ decay away exponentially, representing a transient current distribution that relaxes exponentially as one moves away from the current contacts. The eigenvector $\vec{J}_0$ dictates the current distribution inside the bulk. Solving for its explicit form, one finds $J^{(R)}_0/J^{(L)}_0 = N/(N+M)$: the ratio of currents is proportional to ratio of the number of channels. As expected, the current relaxes into an equilibrium distribution in which the current carried by each channel at an edge is equal.

That the system exhibits a quantized Hall effect can easily be seen from this last result. For any two voltage contacts $n_{1,2}$, which are both far from the current contacts, the transient part of the current distribution is negligibly small [44], so that $\vec{J}_{n_1+1/2} = \vec{J}_{n_2+1/2} = \vec{J}_{n_1-1/2} = \vec{J}_{n_2-1/2}$. It follows that the chemical potentials in these voltage probes must be the same, so that the measured longitudinal resistance will vanish. To find the Hall resistance, we define $J^C_{T(B)}$ as the difference in current carried by each channel on the top (bottom) edge due to currents injected/removed by the contacts far to the right and left of the system. On the top edge, the resulting extra current into a voltage contact is then $\Gamma(2N+M)J^C_T$. An equal current must then exit from the voltage reservoir back into the system. Assuming the reservoir also has $2N+M$ channels, detailed balance requires the probability of tunneling from a reservoir channel back into an edge channel is also Γ. The extra current per channel exiting the reservoir must then be J^C_T, which fixes the change in chemical potential in the reservoir, $\delta\mu_T = hJ^C_T/e^2$. Analogous reasoning fixes the chemical potential change for voltage probes well inside the Hall bar along the bottom edge to be $\delta\mu_B = hJ^C_B/e^2$. Finally, recognizing that the net current down the length of the Hall bar is $I = M(J^C_T - J^C_B) = M\frac{e^2}{h}(\delta\mu_T - \delta\mu_B)$, we arrive at a quantized Hall conductance of $M\frac{e^2}{h}$.

VIII. SUMMARY

In this paper, we have studied a simplified model of surface states in topological insulators. The model allowed us to develop straightforward matching conditions for states on different surfaces, opening the possibility to understand the surface spectra of a variety of mesoscopic systems. Two systems were analyzed in this formalism in detail: a quantum wire of rectangular cross-section, and a slab geometry in the quantum Hall regime.

For the rectangular wire, one finds transverse states with a quantization condition that reflects the helicity of the wave functions: an effective two component spinor follows a circular trajectory as one moves around a closed path around the wire, inducing a phase that prevents gapless modes from appearing in the spectrum. The resulting gap vanishes only as the wire cross-sectional area becomes very large. The application of exchange fields on two of the surfaces changes the topological character of the surface states by inducing a nonvanishing Chern number. This results in chiral states on lateral surfaces that are gapless. In contrast, if the exchange fields on the two surfaces are directed antiparallel, the Chern number vanishes, and chiral states are absent from the spectrum.

We also considered the surface spectrum of a slab in a magnetic field. Landau level states appear on the surfaces perpendicular to the field, which are continuously connected to zero field states on the lateral surfaces [14]. The lateral states have unequal numbers of channels propagating in opposite directions along the slab, in direct analogy with what expects of edge states in the quantized Hall effect. The large number of counterpropagating edge channels spoils the quantum Hall

effect in this system in the ballistic regime. This is due to the existence of unequilibrated populations of the channels on a surface due to the injection of current in the system. We found that processes which restore the populations of the edge modes into local equilibrium, as modeled by floating voltage contacts along the edge, will lead to a quantum Hall effect in the system if voltage measurements are made sufficiently far from the current contacts.

ACKNOWLEDGMENTS

LB acknowledges fruitful discussions with Alfredo Levy Yeyati. Funding for this work was provided by MEC-Spain via grant FIS2012-33521. HAF acknowledges support by the US-NSF through Grant No. DMR-1005035 and by the US-Israel Binational Science Foundation through Grant No. 2012120.

APPENDIX: DIRAC HAMILTONIAN AND METALLIC STATES IN THE $\hat{z}$ SURFACE

In this Appendix, we outline how, starting from the three-dimensional Hamiltonian (3), one obtains the Dirac Hamiltonian describing the surface states of a TI. For concreteness, we discuss the $\hat{z}$ surface but similar derivations can be carried out for other surface orientations. In this surface the system is invariant in the $\hat{x}$ and $\hat{y}$ direction, so that k_x and k_y are good quantum numbers. States localized in the surface with energy in the bulk gap must decay exponentially in the bulk. Moreover, we adopt a vanishing boundary condition [25] right at the surface, $z = 0$. We thus look for wave functions of the form

$$u(k_x,k_y,\lambda_{1,2})\, e^{i(k_x x+k_y y)}(e^{\lambda_1 z} - e^{\lambda_2 z}), \tag{A1}$$

where $\mathrm{Re}\lambda_{1,2} > 0$ and u is the spinor eigenstate of Hamiltonian (3) corresponding to k_x, k_y and $k_z = -i\lambda_{1,2}$. Note one needs to find two *different* values of $\lambda_{1,2}$ with the *same* such spinor [25], in order for all four components of the wave function to vanish at $z = 0$. We are interested in the surface Hamiltonian to lowest nontrivial order in the wave vector; therefore, in the spirit of the $\mathbf{k}\cdot\mathbf{p}$ approximation, we first obtain the eigenstates for $k_x = k_y = 0$, and then write the finite wave-vector Hamiltonian in this basis. Our approach differs from that of Ref. [25] in dropping the k_x and k_y dependence of the basis states, which introduces higher order corrections in the wave vectors. This turns out to be a considerable simplification which allows us to develop relatively simple matching conditions, as well as to introduce a magnetic field in a straightforward way.

Substituting $i\lambda$ for k_z in Eq. (3), the equation $\det[H_{3D} - E\mathbb{I}] = 0$, where $\mathbb{I}$ is the 4×4 unit matrix, fixes the inverse decay length λ. Again ignoring the diagonal term in H_{3D}, this yields the biquadratic equation

$$(E + D_1\lambda^2)^2 = (M_0 + B_1\lambda^2)^2 - A_1^2\lambda^2\,, \tag{A2}$$

which fixes possible values of λ. For each energy it is possible to obtain two solutions $\lambda_{1,2}$ with $\mathrm{Re}\lambda_{1,2} > 0$. The required energy value is found by imposing the condition $u(\lambda_1) = u(\lambda_2)$,

$$[H^{3D}(\lambda_1) - H^{3D}(\lambda_2)]u(\lambda_1) = 0, \tag{A3}$$

which implies a further relation

$$\left(D_1^2 - B_1^2\right)(\lambda_2 + \lambda_1)^2 - A_1^2 = 0\,. \tag{A4}$$

This, together with Eq. (A2), yields an energy eigenvalue $E = \frac{D_1}{B_1}M_0$. Each of the two allowed values of λ furthermore admit two eigenvectors of H_{3D},

$$u^{+\hat{z}} = \frac{1}{\sqrt{2}}\begin{pmatrix}\sqrt{1+\frac{D_1}{B_1}}\\ -i\sqrt{1-\frac{D_1}{B_1}}\\ 0\\ 0\end{pmatrix}, \quad v^{+\hat{z}} = \frac{1}{\sqrt{2}}\begin{pmatrix}0\\ 0\\ \sqrt{1+\frac{D_1}{B_1}}\\ i\sqrt{1-\frac{D_1}{B_1}}\end{pmatrix}. \tag{A5}$$

Finally, we project the three dimensional Hamiltonian (3) in basis states of the form in Eq. (A1), using the spinors defined in Eq. (A5). To lowest order in k_x and k_y, this results in the Dirac Hamiltonian

$$H^{\hat{z}} = \frac{D_1}{B_1}M_0 + A_2\sqrt{1-\frac{D_1^2}{B_1^2}}\begin{pmatrix}0 & ik_x+k_y\\ -ik_x+k_y & 0\end{pmatrix} \tag{A6}$$

as given in the text.

[1] M. Z. Hasan and C. L. Kane, Rev. Mod. Phys. **82**, 3045 (2010).
[2] X.-L. Qi and S.-C. Zhang, Rev. Mod. Phys. **83**, 1057 (2011).
[3] Y. Ando, J. Phys. Soc. Jpn. **82**, 102001 (2013).
[4] L. Xia *et al.*, Nat. Phys. **5**, 398 (2009).
[5] Y. L. Chen *et al.*, Science **325**, 178 (2009).
[6] J. W. McClure, Phys. Rev. **104**, 666 (1956).
[7] P. Cheng, C. Song, T. Zhang, Y. Zhang, Y. Wang, J.-F. Jia, J. Wang, Y. Wang, B.-F. Zhu, X. Chen, *et al.*, Phys. Rev. Lett. **105**, 076801 (2010).
[8] T. Hanaguri, K. Igarashi, M. Kawamura, H. Takagi, and T. Sasagawa, Phys. Rev. B **82**, 081305 (2010).
[9] Y. Jiang, Y. Wang, M. Chen, Z. Li, C. Song, K. He, L. Wang, X. Chen, X. Ma, and Q.-K. Xue, Phys. Rev. Lett. **108**, 016401 (2012).
[10] A. A. Taskin, S. Sasaki, K. Segawa, and Y. Ando, Phys. Rev. Lett. **109**, 066803 (2012).
[11] R. Jackiw, Phys. Rev. D **29**, 2375 (1984).
[12] L. Fu and C. L. Kane, Phys. Rev. B **76**, 045302 (2007).
[13] D.-H. Lee, Phys. Rev. Lett. **103**, 196804 (2009).
[14] O. Vafek, Phys. Rev. B **84**, 245417 (2011).
[15] Y.-Y. Zhang, X.-R. Wang, and X. C. Xie, J. Phys.: Condens. Matter **24**, 015004 (2012).
[16] T. Yokoyama, Y. Tanaka, and N. Nagaosa, Phys. Rev. B **81**, 121401 (2010).
[17] I. Garate and M. Franz, Phys. Rev. Lett. **104**, 146802 (2010).
[18] X.-L. Qi, T. L. Hughes, and S.-C. Zhang, Phys. Rev. B **78**, 195424 (2008).
[19] X.-L. Qi *et al.*, Science **323**, 1184 (2009).
[20] R. Yu *et al.*, Science **329**, 61 (2010).

[21] C.-Z. Chang, J. Zhang, X. Feng, J. Shen, Z. Zhang, M. Guo, K. Li, Y. Ou, P. Wei, L.-L. Wang, *et al*., Science **340**, 167 (2013).
[22] H. Zhang, *et al*., Nat. Phys. **5**, 438 (2009).
[23] C.-X. Liu, X.-L. Qi, H. J. Zhang, X. Dai, Z. Fang, and S.-C. Zhang, Phys. Rev. B **82**, 045122 (2010).
[24] M. Lasia and L. Brey, Phys. Rev. B **86**, 045317 (2012).
[25] P. G. Silvestrov, P. W. Brouwer, and E. G. Mishchenko, Phys. Rev. B **86**, 075302 (2012).
[26] Wen-Yu Shan *et al*., New J. Phys. **12**, 043048 (2010).
[27] H.-Z. Lu, W.-Y. Shan, W. Yao, Q. Niu, and S.-Q. Shen, Phys. Rev. B **81**, 115407 (2010).
[28] J. Linder, T. Yokoyama, and A. Sudbø, Phys. Rev. B **80**, 205401 (2009).
[29] Yi Zhang, Ke He, Cui-Zu Chang, Can-Li Song, Li-Li Wang, Xi Chen, Jin-Feng Jia, Zhong Fang, Xi Dai, Wen-Yu Shan, Shun-Qing Shen, Qian Niu, Xiao-Liang Qi, Shou-Cheng Zhang, Xu-Cun Ma, and Qi-Kun Xue, Nat. Phys. **6**, 584 (2010).
[30] C.-X. Liu, H. J. Zhang, B. Yan, X.-L. Qi, T. Frauenheim, X. Dai, Z. Fang, and S.-C. Zhang, Phys. Rev. B **81**, 041307(R) (2010).
[31] D. Sen and O. Deb, Phys. Rev. B **85**, 245402 (2012).
[32] O. Deb, A. Soori, and D. Sen, arXiv:1401.1027.
[33] J. Londergan, J. Carini, and D. Murdock, *Binding and Scattering in Two-Dimensional Systems* (Springer-Verlag, New York, 1999).
[34] A. Iyengar, T. Luo, H. A. Fertig, and L. Brey, Phys. Rev. B **78**, 235411 (2008).
[35] In general, the surface states can depend on the in-plane momentum, but this will plays no role in what follows.
[36] T. Luo, A. P. Iyengar, H. A. Fertig, and L. Brey, Phys. Rev. B **80**, 165310 (2009).
[37] R. Egger, A. Zazunov, and A. L. Yeyati, Phys. Rev. Lett. **105**, 136403 (2010).
[38] A. Kundu, A. Zazunov, A. L. Yeyati, T. Martin, and R. Egger, Phys. Rev. B **83**, 125429 (2011).
[39] I. S. Gradshteyn and I. M. Ryzhik, *Table of Integrals, Series, and Products*, 5th ed. (Academic Press, San Diego Ca., 1994).
[40] Similar results may be found in Ref. [14].
[41] M. Ramezani Masir, P. Vasilopoulos, A. Matulis, and F. M. Peeters, Phys. Rev. B **77**, 235443 (2008).
[42] J. G. Analytis *et al*., Nat. Phys. **6**, 960 (2010).
[43] M. Büttiker, Phys. Rev. B **32**, 1846 (1985).
[44] J. Wang, B. Lian, H. Zhang, and S.-C. Zhang, Phys. Rev. Lett. **111**, 086803 (2013).